Alexandria Engineering Journal (2022) 61, 7605–7617

HOSTED BY

ELSEVIER

Alexandria University

Alexandria Engineering Journal

www.elsevier.com/locate/aej
www.sciencedirect.com

Magnetohydrodynamic and viscous dissipation effects on radiative heat transfer of non-Newtonian fluid flow past a nonlinearly shrinking sheet: Reiner–Philippoff model

Najiyah Safwa Khashi'ie [a], Iskandar Waini [a,*], Abdul Rahman Mohd Kasim [b], Nurul Amira Zainal [a], Anuar Ishak [c], Ioan Pop [d]

[a] *Fakulti Teknologi Kejuruteraan Mekanikal dan Pembuatan, Universiti Teknikal Malaysia Melaka, Hang Tuah Jaya, 76100 Durian Tunggal, Melaka, Malaysia*
[b] *Centre for Mathematical Sciences, College of Computing & Applied Sciences, Universiti Malaysia Pahang, Lebuhraya Tun Razak, Gambang 26300, Pahang, Malaysia*
[c] *Department of Mathematical Sciences, Faculty of Science and Technology, Universiti Kebangsaan Malaysia, 43600 UKM Bangi, Selangor, Malaysia*
[d] *Department of Mathematics, Babeş-Bolyai University, 400084 Cluj-Napoca, Romania*

Received 28 October 2021; revised 9 December 2021; accepted 2 January 2022
Available online 13 January 2022

KEYWORDS

Non-Newtonian fluid;
Reiner–Philippoff fluid;
Shrinking sheet;
Viscous dissipation;
MHD;
Dual solutions

Abstract Heat transfer is an important process in many engineering, industrial, residential, and commercial buildings. Thus, this study aims to analyse the effect of MHD and viscous dissipation on radiative heat transfer of Reiner–Philippoff fluid flow over a nonlinearly shrinking sheet. By adopting appropriate similarity transformations, the partial derivatives of multivariable differential equations are transformed into the similarity equations of a particular form. The resulting mathematical model is elucidated in MATLAB software using the bvp4c technique. To determine the impact of physical parameters supplied into the problem, the results are shown in the form of tables and graphs. The findings reveal that the heat transfer rate reduces as the Eckert number and radiation parameter are introduced in the operating fluid. However, increasing the magnetic parameter raises both the skin friction coefficient and the local Nusselt number, which impulsively improves the heat transfer performance. The suction effect has a noticeable influence on the Reiner–Philippoff fluid, since increasing the suction parameter's value is seen to enhance the skin friction coefficient and the heat transfer performance. The dual solutions are established, leading to the stability analysis that supports the first solution's validity.

* Corresponding author.
E-mail address: iskandarwaini@utem.edu.my (I. Waini).

Peer review under responsibility of Faculty of Engineering, Alexandria University.

https://doi.org/10.1016/j.aej.2022.01.014
1110-0168 © 2022 THE AUTHORS. Published by Elsevier BV on behalf of Faculty of Engineering, Alexandria University

Nomenclature

a	constant
B_0	constant magnetic strength (T)
$B(x)$	magnetic field (T)
C_f	skin friction coefficient
C_p	specific heat at constant pressure ($Jkg^{-1}K^{-1}$)
(ρC_p)	heat capacitance of the fluid ($JK^{-1}m^{-3}$)
Ec	Eckert number
f	dimensionless stream function
g	dimensionless shear stress
F, G, H	arbitrary functions
k	thermal conductivity of the fluid ($Wm^{-1}K^{-1}$)
k^*	Rosseland mean absorption coefficient (m^{-1})
M	magnetic parameter
Nu_x	local Nusselt number
Pr	Prandtl number
q_w	surface heat flux (Wm^{-2})
q_r	radiative heat flux (Wm^{-2})
R	thermal radiation parameter
Re_x	local Reynolds number
S	mass flux parameter
t	time (s)
T	fluid temperature (K)
T_∞	ambient temperature (K)
T_0	reference temperature (K)
u, v	velocity component in the x- and y- directions (ms^{-1})
u_w	velocity of the surface (ms^{-1})
v_w	velocity of the mass flux (ms^{-1})
x, y	Cartesian coordinates (m)

Greek symbols

α	eigenvalue
ε	stretching/shrinking parameter
γ	Bingham number
η	similarity variable
θ	dimensionless temperature
τ	shear stress ($kgm^{-1}s^{-2}$)
τ_w	wall shear stress ($kgm^{-1}s^{-2}$)
τ_s	reference skin friction ($kgm^{-1}s^{-2}$)
λ	Reiner–Philippoff fluid parameter
μ_0	dynamic viscosity at zero shear stress ($kgm^{-1}s^{-1}$)
μ_∞	dynamic viscosity as the shear stress becomes large ($kgm^{-1}s^{-1}$)
ν	kinematic viscosity of the fluid (m^2s^{-1})
ρ	density of the fluid (kgm^{-3})
σ	electric conductivity (S/m)
σ^*	Stefan-Boltzmann constant ($Wm^{-2}K^{-4}$)
Γ	dimensionless time variable
ψ	stream function

Superscript

$'$	differentiation with respect to η

1. Introduction

The progress in the research of fluid flow is rapid growth due to the robust development in industrial applications. This situation happened due to the demand in getting the best output in certain processes where the fluid motions are having the ability for most of the transport and mixing of materials. Such a situation is frequently established in food industries, beverages making, the oil industry, gasoline engineering, pharmaceuticals, chemicals manufacturing, and plastics sectors. In the process of excavating the best method to develop the best end product, the classical fluid like water which is also classified under Newtonian type is no more valid in fulfilling the industrial demands due to indecisiveness in describing the properties of fluid's material. Hence, the various subclass of non-Newtonian fluids with different features like shear rate-dependent viscosity and normal stress, are widely used to counter the limitation. Unlike the Newtonian fluid model which is based on the linear relationship between strain and stress tensors, the non-Newtonian fluid models are observed based on their behavior either shear thickening (dilatant) or shear thinning (pseudo-plasticity). The shear-thickening implies the increasing viscosity with increasing shear rate, while the shear-thinning fluid exhibits the Newtonian fluid's behavior when the shear rate is very low/high values. There are many proposed models exhibit with both shear thickening and thinning behaviors like the Reiner–Philippoff fluid, the Sisko fluid, Powell–Eyring fluid, Carreau–Yasuda fluid, the Carreau viscosity fluid [1].

The ability in unveiling the Newtonian fluid (shear stress approaches zero) or non-Newtonian fluid (other values of shear stress) has made the Reiner–Philippoff fluid model be the center of attraction among the investigators. The contribution on the Reiner–Philippoff's model has been endorsed by Kapur and Gupta [2] and Cavatorta and Tonini [3] in the report under topic; the flow of Reiner-Philippoff fluid inside a channel using Karman-Pohlhausen's method and computation of the velocity profiles for non-Newtonian Reiner–Philippoff, Ellis, Ostwald de Waele, generalized Bingham and Prandtl Eyring fluids respectively. Besides, the investigation was also conducted on the flow over a stretching surface in non-Newtonian fluids owing to their significance in many engineering and industrial processes. Prior analysis has been performed by Hansen and Na [4] which discovered the similarity solutions only exist when the non-Newtonian fluids (any model) flow over a 90° wedge. Advanced, Na [5] extended this study by considering two cases which are the non-similar solution for the Blasius flow and the similarity solution for the flow over a 90° wedge. The report on similarity solutions for the boundary layer flow in a three-dimensional system using a general non-Newtonian fluid model was found in a document by Timol and Kalthia [6], Patel and Timol [7], and Patil et al. [8]. The exploration on boundary layer flow of Reiner–Philippoff fluids induced by a stretching 90° wedge was dedicated by Yam et al. [9] where the stability analysis was highlighted and the final conclusion revealed there were no multiple solutions exist. Another attempt on investigating Reiner–Philippoff fluids has been accomplished by Reddy

et al. [10,11], Ahmad [12], Ahmad et al. [13], Kumar et al. [14], Xiong et al. [15], and Sajid et al. [16,17]. On the other hand, other non-Newtonian fluid models subject to various geometries have been investigated and analyzed by Kefayati [18–20], Kefayati and Huilgol [21], Kefayati and Tang [22,23], Nandi and Kumbhakar [24], Sharma et al. [25], Kumar et al. [26] and Abegunrin et al. [27].

The progress in discovering the model of fluid that can contribute to enhancing the flow properties has always been the main focus. The endeavors do not limit to proposing the new model's formulation but also considering the existing ideas and studying their appropriateness to the proposed model. Among the available additional extension on the fluid flow problem, the MHD and viscous dissipation effects are among the applicable elements that should be deliberated. It is acknowledged the fluid with MHD has the capability to regulate the flow separation and become the agent of manipulating the heat transfer of certain fluids. Meanwhile, the viscous dissipation is attributed during the movement of fluid particles where the viscosity of fluid converted the kinetic energy into thermal energy. These two effects are independent of each other and can be considered separately. As reported in the literature, the term MHD was happened to be in the momentum equation while viscous dissipation in the energy equation. The simultaneous effects of MHD and heat source/sink were numerically studied by Seth et al. [28] for a viscous flow. Further, Seth and Mandal [29] analyzed the electromagnetohydrodynamic (EMHD) flow subject to a nonlinearly stretching sheet with variable thickness. Mishra et al. [30] observed the existence of multiple solutions when considering MHD flow with thermal radiation and viscous dissipation effects over a stretching/shrinking sheet. Babu and Sandeep [31] found that the magnetic and radiation parameters could enhance the thermal boundary layer. The discovery of MHD towards the flow field is once carried out by Asimoni et al. [32] where the focus is under the two-dimensional laminar flow of non-Newtonian power-law nanofluid, while Zokri et al. [33] examined the problem of MHD embedded in Jeffrey fluid. Very recent findings on this topic are led by Waini et al. [34] and Pop et al. [35] where the hybrid nanofluid is the main focus and the flow is assumed to stream over a shrinking sheet. Some other documents on the MHD discovery are acknowledged in the reports by Aurangzaib et al. [36,37], Ariffin et al. [38,39], Nandi et al. [40], Ghiasi et al. [41], and Gajjela et al. [42].

A recent topic of interest is the analysis of the dual solution with its stability for the boundary layer flow in various fluids and surfaces. The concern is to choose the physical solution (s) among the potential available solutions. The dual solutions frequently exist for the case of fluid motion induced by a shrinking sheet as early studied by Miklavčič and Wang [43] for a Newtonian fluid model. The generation of shrinking flow with an appropriate suction strength contributed to the existence of dual similarity solutions. In certain cases, there are possibilities that multiple solutions (more than two) exist which have been explored by Turkyilmazoglu [44], Lund et al. [45], and Yahaya et al. [46]. Moreover, the flow analysis due to the shrinking surfaces have been conducted and discussed by Yahaya et al. [47,48] for non-Newtonian fluids and Waini et al. [49–51], Naramgari and Sulochana [52], Anuar et al. [53], Zainal et al. [54,55], Wahid et al. [56–58] and Bhattacharyya et al. [59] for other fluids.

Motivated from the existing studies while fulfilling the research gap, the main strength of this numerical study is the contribution of dual solutions and stability analysis for non-Newtonian radiative Reiner–Philippoff fluid flow past a nonlinearly shrinking sheet with the inclusion of MHD and viscous dissipation. A previous paper by Yam et al. [9] only considered the unique solution of Reiner–Philippoff fluid flow subject to a wedge geometry. Meanwhile, this present paper focuses on the observation of dual solutions including the conduct of stability analysis for the nonlinear shrinking sheet with several physical factors. To the best of the authors' knowledge, the study on the non-Newtonian radiative Reiner–Philippoff fluid flow past a nonlinearly shrinking sheet embedded with the MHD and viscous dissipation has not been considered and therefore, this endeavor is significant as a future reference for the selected topic. For the methodology, the efficient bvp4c solver in the Matlab software is used to solve the reduced ordinary differential equations. The similarity solutions are graphically displayed and discussed for the skin friction coefficient and thermal distribution including the velocity and temperature profiles. We strongly believe that this numerical study can attract other researchers from various backgrounds.

2. Mathematical formulation

Consider the flow of Reiner–Philippoff fluid past a shrinking sheet as shown in Fig. 1. Here, the surface velocity is $u_w(x) = ax^{1/3}$ with $a > 0$. In addition, the mass flux velocity $v_w(x)$ is considered to represent the surface permeability. Besides, the surface temperature is $T_w(x) = T_\infty + T_0 x^{2/3}$ with the ambient T_∞ and the reference T_0 temperatures are constant [60]. The magnetic field $B(x)$ is transversely applied along the y-axis with $B(x) = B_0 x^{-1/3}$ where B_0 is constant magnetic strength [14]. Furthermore, the radiative heat flux $q_r = -(4\sigma^*/3k^*)(\partial T^4/\partial y)$ is also considered. Here, k^* and σ^* signifies the Rosseland mean absorption coefficient and the Stefan-Boltzmann constant and given that $T^4 \cong 4T_\infty^3 T - 3T_\infty^4$ [61]. In addition, the viscous dissipation and the Joule heating effects are employed [62]. Therefore, the governing equations can be written as [10,14,62]:

$$\frac{\partial u}{\partial x} + \frac{\partial v}{\partial y} = 0 \tag{1}$$

$$\frac{\partial u}{\partial y} = \frac{\tau}{\mu_\infty + \frac{\mu_0 - \mu_\infty}{1+\left(\frac{\tau}{\tau_s}\right)^2}} \tag{2}$$

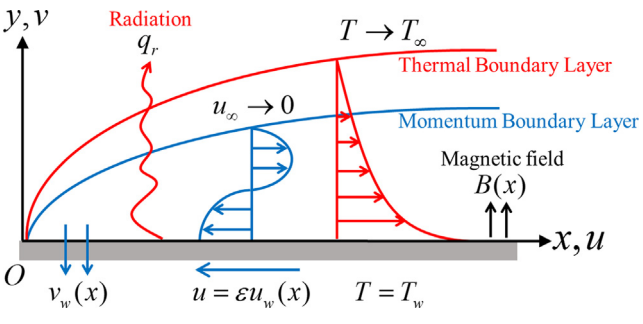

Fig. 1 Flow configuration.

$$u\frac{\partial u}{\partial x}+v\frac{\partial u}{\partial y}=\frac{1}{\rho}\frac{\partial \tau}{\partial y}-\frac{\sigma}{\rho}B^2u \tag{3}$$

$$u\frac{\partial T}{\partial x}+v\frac{\partial T}{\partial y}=\left(\frac{k}{\rho C_p}+\frac{16\sigma^* T_\infty^3}{3(\rho C_p)k^*}\right)\frac{\partial^2 T}{\partial y^2}+\frac{\mu}{\rho C_p}\left(\frac{\partial u}{\partial y}\right)^2+\frac{\sigma}{\rho C_p}B^2u^2 \tag{4}$$

subject to:

$$u=\varepsilon u_w(x),\ \ v=v_w(x),\ \ T=T_w(x)\ \text{ at }\ y=0;\qquad u\to 0,\ \ T\to T_\infty\ \text{ as }\ y\to\infty \tag{5}$$

where ρ is the fluid density, σ is the electric conductivity, ρC_p is the heat capacity, k is the thermal conductivity, T is the temperature, and (u,v) be the velocity components in the (x,y) direction. Besides, τ is the shear stress of the Reiner–Philippoff fluid model with the reference shear stress τ_s, the limiting dynamic viscosity μ_∞, and the zero-shear dynamic viscosity μ_0 [9].

The similarity solutions are only existed by employing the similarity transformation as follows [9]:

$$\psi=\sqrt{av}x^{2/3}f(\eta),\ \ \tau=\rho\sqrt{a^3v}g(\eta),\ \ \theta(\eta)=\frac{T-T_\infty}{T_w-T_\infty},\qquad \eta=\frac{y}{x^{1/3}}\sqrt{\frac{a}{v}} \tag{6}$$

where the stream function ψ is defined by $u=\partial\psi/\partial y$ and $v=-\partial\psi/\partial x$. Then:

$$u=ax^{1/3}f'(\eta),\quad v=-\sqrt{av}x^{-1/3}\left(\frac{2}{3}f(\eta)-\frac{1}{3}\eta f'(\eta)\right) \tag{7}$$

By setting $\eta=0$, the wall mass flux velocity becomes:

$$v_w(x)=-\frac{2}{3}\sqrt{av}x^{-1/3}S \tag{8}$$

where $f(0)=S$ signify the constant mass flux parameter with $S<0$ and $S>0$ are for injection and suction, respectively, while $S=0$ denote the impermeable surface, and $v=\mu_\infty/\rho$ is the fluid kinematic viscosity. Then, on using Eqs. (6) and (7), the similarity equations are obtained as follows:

$$g=f''\left(\frac{\lambda\gamma^2+g^2}{\gamma^2+g^2}\right) \tag{9}$$

$$g'+\frac{2}{3}ff''-\frac{1}{3}f'^2-Mf'=0 \tag{10}$$

$$\frac{1}{\Pr}\left(1+\frac{4}{3}R\right)\theta''+\frac{2}{3}(f\theta'-f'\theta)+Ecf''^2+EcMf'^2=0 \tag{11}$$

subject to:

$$f(0)=S,\ \ f'(0)=\varepsilon,\ \ \theta(0)=1;\qquad f'(\eta)\to 0,\ \ \theta(\eta)\to 0\ \ as\ \ \eta\to\infty \tag{12}$$

with the Reiner–Philippoff fluid parameter λ, the Bingham number γ, the magnetic parameter M, the Eckert number Ec, the Prandtl number Pr, and the thermal radiation parameter R, defined by:

$$\lambda=\frac{\mu_0}{\mu_\infty},\ \ \gamma=\frac{\tau_s}{\rho\sqrt{a^3v}},\ \ M=\frac{\sigma}{\rho a}B_0^2,\ \ Ec=\frac{a^2}{T_0C_p},\qquad \Pr=\frac{\mu C_p}{k},\ \ R=\frac{4\sigma^* T_\infty^3}{kk^*} \tag{13}$$

Note that, $\lambda=1$ is for the Newtonian (viscous) fluid case, while $\lambda<1$ and $\lambda>1$ represent the shear thickening (dilatant) fluid and the shear-thinning (pseudoplastic) fluid cases. Besides,$\varepsilon=0$ denotes the static sheet, while $\varepsilon>0$ and $\varepsilon<0$ signify the stretching and shrinking sheet, respectively.

The coefficient of the skin friction C_f and the local Nusselt number Nu_x are given as:

$$C_f=\frac{\tau_w}{\rho\ u_w^2},\qquad Nu_x=\frac{xq_w}{k(T_w-\ T_\infty)} \tag{14}$$

where

$$\tau_w=\rho\sqrt{a^3v}(g(\eta))_{y=0},\qquad q_w=-\ k\left(\frac{\partial T}{\partial y}\right)_{y=0}+(q_r)_{y=0} \tag{15}$$

Here, τ_w denotes the value of τ on $y=0$ and q_w is the surface heat flux. On using Eqs. (14) and (15), one gets:

$$\mathrm{Re}_x^{1/2}C_f=g(0),\qquad \mathrm{Re}_x^{-1/2}Nu_x=-\left(1+\frac{4}{3}R\right)\theta'(0) \tag{16}$$

where $\mathrm{Re}_x=u_w(x)x/v$ is the local Reynolds number.

3. Stability analysis

The dual solutions are examined to test their stability by employing stability analysis [63,64]. First, consider the semi-similar variables as follows [9]:

$$\psi=\sqrt{av}x^{2/3}f(\eta,\Gamma),\ \ \tau=\rho\sqrt{a^3v}g(\eta,\Gamma),\ \ \theta(\eta,\Gamma)=\frac{T-T_\infty}{T_w-T_\infty},\ \ \eta=\frac{y}{x^{1/3}}\sqrt{\frac{a}{v}},\ \ \Gamma=\frac{a}{x^{2/3}}t \tag{17}$$

where Γ is the dimensionless time variable, and given that:

$$u=ax^{1/3}\tfrac{\partial f}{\partial\eta}(\eta,\Gamma),\qquad v=-\sqrt{av}x^{-1/3}\left(\tfrac{2}{3}f(\eta,\Gamma)-\tfrac{1}{3}\eta\tfrac{\partial f}{\partial\eta}(\eta,\Gamma)-\tfrac{2}{3}\Gamma\tfrac{\partial f}{\partial\Gamma}(\eta,\Gamma)\right) \tag{18}$$

Next, based on Eqs. (3) and (4), consider the following unsteady flow:

$$\frac{\partial u}{\partial t}+u\frac{\partial u}{\partial x}+v\frac{\partial u}{\partial y}=\frac{1}{\rho}\frac{\partial \tau}{\partial y}-\frac{\sigma}{\rho}B^2u \tag{19}$$

$$\frac{\partial T}{\partial t}+u\frac{\partial T}{\partial x}+v\frac{\partial T}{\partial y}=\left(\frac{k}{\rho C_p}+\frac{16\sigma^* T_\infty^3}{3(\rho C_p)k^*}\right)\frac{\partial^2 T}{\partial y^2}+\frac{\mu}{\rho C_p}\left(\frac{\partial u}{\partial y}\right)^2+\frac{\sigma}{\rho C_p}B^2u^2 \tag{20}$$

while Eqs. (1) and (2) remain unchanged. Then, on using Eqs. (17) and (18), one obtains:

$$g=\frac{\partial^2 f}{\partial\eta^2}\left(\frac{\lambda\gamma^2+g^2}{\gamma^2+g^2}\right) \tag{21}$$

$$\frac{\partial g}{\partial \eta}+\frac{2}{3}f\frac{\partial^2 f}{\partial \eta^2}-\frac{1}{3}\left(\frac{\partial f}{\partial \eta}\right)^2-M\frac{\partial f}{\partial \eta}-\frac{\partial^2 f}{\partial \eta \partial \Gamma}-\frac{2}{3}\Gamma\left(\frac{\partial f}{\partial \Gamma}\frac{\partial^2 f}{\partial \eta^2}-\frac{\partial f}{\partial \eta}\frac{\partial^2 f}{\partial \eta \partial \Gamma}\right)=0 \tag{22}$$

$$\frac{1}{\mathrm{Pr}}\left(1+\frac{4}{3}R\right)\frac{\partial^2 \theta}{\partial \eta^2}+\frac{2}{3}\left(f\frac{\partial \theta}{\partial \eta}-\frac{\partial f}{\partial \eta}\theta\right)+Ec\left(\frac{\partial^2 f}{\partial \eta^2}\right)^2+EcM\left(\frac{\partial f}{\partial \eta}\right)^2-\frac{\partial \theta}{\partial \Gamma}-\frac{2}{3}\Gamma\left(\frac{\partial f}{\partial \Gamma}\frac{\partial \theta}{\partial \eta}-\frac{\partial f}{\partial \eta}\frac{\partial \theta}{\partial \Gamma}\right)=0 \tag{23}$$

subject to:

$$\begin{aligned} &f(0,\Gamma)-\tfrac{2}{3}\Gamma\tfrac{\partial f}{\partial \Gamma}(0,\Gamma)=S,\ \ \tfrac{\partial f}{\partial \eta}(0,\Gamma)=\varepsilon,\ \ \theta(0,\Gamma)=1;\\ &\tfrac{\partial f}{\partial \eta}(\eta,\Gamma)\to 0,\ \ \theta(\eta,\Gamma)\to 0\ \text{ as }\ \eta\to\infty \end{aligned} \tag{24}$$

Then, consider the perturbation function [64]:

$$\begin{aligned} f(\eta,\Gamma)&=f_0(\eta)+e^{-\alpha\Gamma}F(\eta,\Gamma),\\ g(\eta,\Gamma)&=g_0(\eta)+e^{-\alpha\Gamma}G(\eta,\Gamma),\\ \theta(\eta,\Gamma)&=\theta_0(\eta)+e^{-\alpha\Gamma}H(\eta,\Gamma) \end{aligned} \tag{25}$$

where $F(\eta,\Gamma)$, $G(\eta,\Gamma)$, and $H(\eta,\Gamma)$ are arbitrary functions and relatively small than $f_0(\eta)$, $g_0(\eta)$, and $\theta_0(\eta)$, and α denotes the eigenvalue. Here, Eq. (25) is employed to obtain the eigenvalue problems of Eqs. (21)–(23). By setting $\Gamma=0$, then $F(\eta,\Gamma)=F_0(\eta)$, $G(\eta,\Gamma)=G_0(\eta)$, and $H(\eta,\Gamma)=H_0(\eta)$. Therefore, after linearization, the eigenvalue problems are:

$$G_0=F_0''\left(\frac{\lambda\gamma^2+g_0^2}{\gamma^2-2f_0''g_0+3g_0^2}\right) \tag{26}$$

$$G_0'+\frac{2}{3}\left(f_0F_0''+f_0''F_0\right)-\frac{2}{3}f_0'F_0'-MF_0'+\alpha F_0'=0 \tag{27}$$

$$\frac{1}{\mathrm{Pr}}\left(1+\frac{4}{3}R\right)H_0''+\frac{2}{3}\left(f_0H_0'+\theta_0'F_0\right)-\frac{2}{3}\left(f_0'H_0+\theta_0F_0'\right)+2Ecf_0''F_0''+2EcMf_0'F_0'+\alpha H_0=0 \tag{28}$$

subject to:

$$\begin{aligned} &F_0(0)=0,\ \ F_0'(0)=0,\ \ H_0(0)=0;\\ &F_0'(\eta)\to 0,\ \ H_0(\eta)\to 0\ \text{ as }\ \eta\to\infty \end{aligned} \tag{29}$$

Here, to obtain α from Eqs. (26)–(28), $F_0'(\eta)\to 0$ as $\eta\to\infty$ in Eq. (29) is replaced by $F''(0)=1$ [65].

4. Results and discussion

This section provides a discussion of the results obtained from the numerical computation. Eqs. (9)–(12) are solved by employing a bvp4c package in the MATLAB software [66].

Table 2 Values of $-\theta'(0)$ for different Ec and Pr when $\varepsilon=\lambda=\gamma=R=1$ and $S=M=0$.

Ec	Pr	Bataller [60]	Present Result
0	3	0.97887	0.978932
0.2		0.91586	0.915936
1		0.66393	0.663954
1.5		0.50639	0.506466
0.2	0.71	0.35480	0.354736
	2	0.71646	0.716577
	3	0.91586	0.915936
	10	1.79029	1.790431

The analysis involved discussions on the effect of several physical parameters that arise in the proposed model where the outputs of the computation are presented in graphical and tabular forms. To validate the reliability of the present model, a direct comparative study is performed with the skin friction values $f''(0)$ obtained by Cortell [67], Ferdows et al. [68], and Waini et al. [69] where the present model can be reduced to the equations that once presented in their investigations. Further validation of the temperature gradient $-\theta'(0)$ is made in Table 2 between present values and those by Bataller [60] for different Ec and Pr. The results of comparison as presented in Tables 1 and 2 show an excellent agreement. This gives confidence to the validity and accuracy of the present mathematical formulation and the numerical results.

Figs. 2 and 3 are presented to get an insight into the effect of λ and γ towards the variations of $\mathrm{Re}_x^{1/2}C_f$ and $Re_x^{-1/2}Nu_x$ when $\varepsilon=1$, $S=M=Ec=R=0$ and $\mathrm{Pr}=10$. An upsurge of λ contributed to the declining of $\mathrm{Re}_x^{1/2}C_f$ and increasing of $Re_x^{-1/2}Nu_x$. At $\lambda=1$ (Newtonian fluid), the values of $\mathrm{Re}_x^{1/2}C_f$ and $Re_x^{-1/2}Nu_x$ when $\gamma=0.3,0.5,2$ remain unchanged such that $\mathrm{Re}_x^{1/2}C_f=-0.677648$ and $Re_x^{-1/2}Nu_x=3.067894$ (see Table 3). Further, with the rising values of γ, it is obviously shown that the quantity of $\mathrm{Re}_x^{1/2}C_f$ increases when $\lambda<1$ (shear-thickening fluid) and decreases when $\lambda>1$ (shear-thinning fluid) while the contradict results are obtained for the thermal rate. In addition, the computed values of $\mathrm{Re}_x^{1/2}C_f$ and $\mathrm{Re}_x^{-1/2}Nu_x$ with various values of λ and γ are tabulated in Table 3 for future references.

Table 4 provides the values of $\mathrm{Re}_x^{1/2}C_f$ and $\mathrm{Re}_x^{-1/2}Nu_x$ for various values of the dimensionless physical parameters. At a certain fixed value for the inspected parameters ($\varepsilon=-1, S=2.4, \lambda=1.5, M=0.01$, $\gamma=Ec=0.1$, $R=3$, and $\mathrm{Pr}=10$), it is perceived that the values of $\mathrm{Re}_x^{1/2}C_f$ increase for the rising in S and M, while they are decline with the addi-

Table 1 Values of $f''(0)$ for different S when $\varepsilon=\lambda=\gamma=1$ and $M=0$.

S	Cortell [67]	Ferdows et al. [68]	Waini et al. [69]	Present Result
−0.5	−0.518869	−0.518869	−0.518869	−0.518869
0	−0.677647	−0.677648	−0.677648	−0.677648
0.5	−0.873627	−0.873643	−0.873643	−0.873643

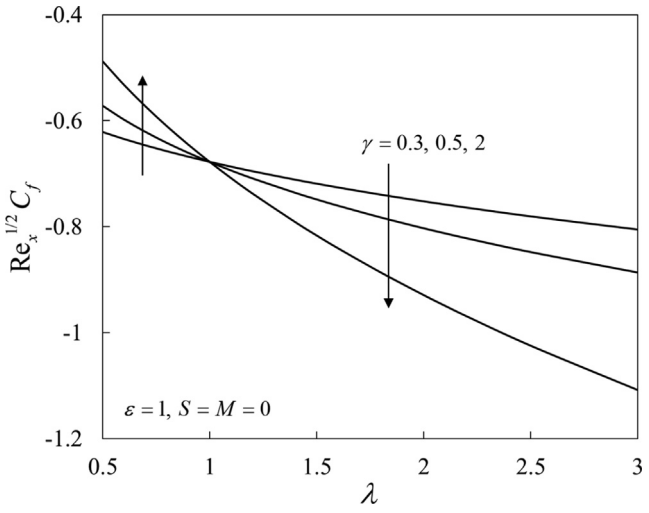

Fig. 2 Skin friction coefficient $Re_x^{1/2} C_f$ vs λ for various values of γ.

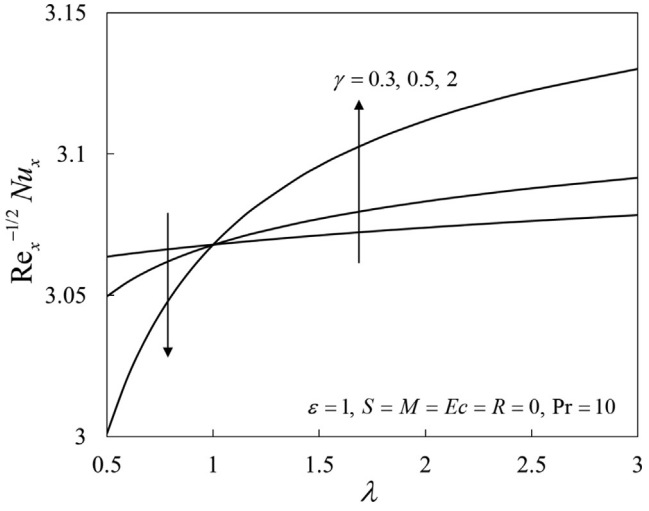

Fig. 3 Local Nusselt number $Re_x^{-1/2} Nu_x$ vs λ for various values of γ.

tion of ε, λ, and γ. The changes in Ec, R, and Pr do not affect the values of $\mathrm{Re}_x^{1/2} C_f$ since these parameters are independent of the momentum equation. The values of $\mathrm{Re}_x^{-1/2} Nu_x$ (thermal rate) boost with the increment of ε, S, M, and Pr, whereas they are showing a downturn trend with the accession of λ, γ, Ec, and R. The dominance of stretching flow, suction, magnetic parameter, and high Prandtl number tends to release the energy to the flow while the existence of Reiner–Philippoff fluid parameter, the Bingham number, Eckert number, and radiation parameter retards the flow energy.

Figs. 4 and 5 illustrate the variations of $\mathrm{Re}_x^{1/2} C_f$ and $\mathrm{Re}_x^{-1/2} Nu_x$ against the shrinking parameter ε for three different fluids: shear-thickening ($\lambda < 1$), Newtonian ($\lambda = 1$), and shear-thinning ($\lambda > 1$). From these figures, the shear-thickening fluid ($\lambda = 0.8$) extends the solution's domain of ε with the critical values of $\varepsilon_{c1} = -1.1567$, followed by the Newtonian fluid ($\lambda = 1$) with $\varepsilon_{c2} = -1.1352$, and the shear-thinning fluid ($\lambda = 1.5$) with $\varepsilon_{c3} = -1.0798$. This signifies the important role of the non-Newtonian fluid from the shear-thickening subclass in the boundary layer separation. The critical value is usually distinguished as the separation value from laminar to turbulent boundary layer flow. Further, both $\mathrm{Re}_x^{1/2} C_f$ and $\mathrm{Re}_x^{-1/2} Nu_x$ deteriorate with an upsurge of λ.

The plots of the skin friction coefficient $\mathrm{Re}_x^{1/2} C_f$ and the local Nusselt number $\mathrm{Re}_x^{-1/2} Nu_x$ against S for diverse values of λ,M, Ec, and R are illustrated in Figs. 6–11. The suction parameter is one of the contributing factors in the generation of similarity solutions. It is noticed that the dual similarity solutions exist for $\mathrm{Re}_x^{1/2} C_f$ and $\mathrm{Re}_x^{-1/2} Nu_x$ up to a minimum/-critical value of the suction parameter called S_c where beyond these values, no other solutions are reached. The enlargement of S_c is requirable for the addition of Reiner–Philippoff fluid parameter λ such that $S_{c1} = 2.2215$ ($\lambda = 0.8$), $S_{c2} = 2.2499$ ($\lambda = 1$), and $S_{c3} = 2.3163$ ($\lambda = 1.5$). This implies the shear-thinning fluid ($\lambda > 1$) obligates more suction strength to induce the fluid motion yet produces two solutions. Besides, the values of $\mathrm{Re}_x^{1/2} C_f$ and $\mathrm{Re}_x^{-1/2} Nu_x$ lessen with the increment of λ as presented in Figs. 6 and 7. From the physical point of view, larger values of λ create obstacles to the shear-thinning effect which reduce the contact of fluid to surfaces and yield fewer drag forces.

Contrarily, Figs. 8 and 9 show that as the magnetic parameter M increases, less suction strength is needed in generating the solutions where $S_{c1} = 2.3422$ ($M = 0$), $S_{c2} = 2.3163$

Table 3 Values of $\mathrm{Re}_x^{1/2} C_f$ and $\mathrm{Re}_x^{-1/2} Nu_x$ for λ and γ when $\varepsilon = 1$, $S = M = Ec = R = 0$, and $\mathrm{Pr} = 10$.

λ	$\mathrm{Re}_x^{1/2} C_f$			$\mathrm{Re}_x^{-1/2} Nu_x$		
	$\gamma = 0.3$	$\gamma = 0.5$	$\gamma = 2$	$\gamma = 0.3$	$\gamma = 0.5$	$\gamma = 2$
0.5	−0.621590	−0.571308	−0.487759	3.063624	3.049700	3.001094
0.8	−0.657721	−0.641512	−0.610295	3.066347	3.062447	3.049366
1	−0.677648	−0.677648	−0.677648	3.067894	3.067894	3.067894
1.2	−0.695334	−0.708625	−0.737428	3.069294	3.072134	3.081279
1.5	−0.718770	−0.748420	−0.816691	3.071182	3.077117	3.095768
2	−0.752030	−0.802982	−0.929234	3.073917	3.083286	3.111775
2.5	−0.780308	−0.848005	−1.024871	3.076280	3.087925	3.122407
3	−0.805100	−0.886657	−1.108574	3.078370	3.091646	3.130094

Table 4 Values of $\mathrm{Re}_x^{1/2}C_f$ and $\mathrm{Re}_x^{-1/2}Nu_x$ for various values of physical parameters.

ε	S	λ	γ	M	Ec	R	Pr	$\mathrm{Re}_x^{1/2}C_f$	$\mathrm{Re}_x^{-1/2}Nu_x$
−1	2.4	1.5	0.1	0.01	0.1	3	10	1.127876	11.277762
0.5								−0.875647	17.059217
1								−1.870635	17.490042
−1	2.38							1.099379	11.047620
	2.35							1.050061	10.666508
	2.32							0.974659	10.155402
	2.4	0.8						1.161349	11.406684
		1						1.153161	11.373878
		1.2						1.144044	11.338411
		1.5	0.15					1.100107	11.170018
			0.18					1.075828	11.076295
			0.2					1.052414	10.987043
			0.1	0				1.102980	11.239276
				0.015				1.138984	11.293718
				0.02				1.149432	11.308099
				0.01	0			1.127876	12.003672
					0.15			1.127876	10.914808
					0.2			1.127876	10.551853
					0.1	1		1.127876	13.305740
						2		1.127876	12.249361
						2.5		1.127876	11.751529
						3	5	1.127876	4.256010
							7	1.127876	6.949639
							8	1.127876	8.366637

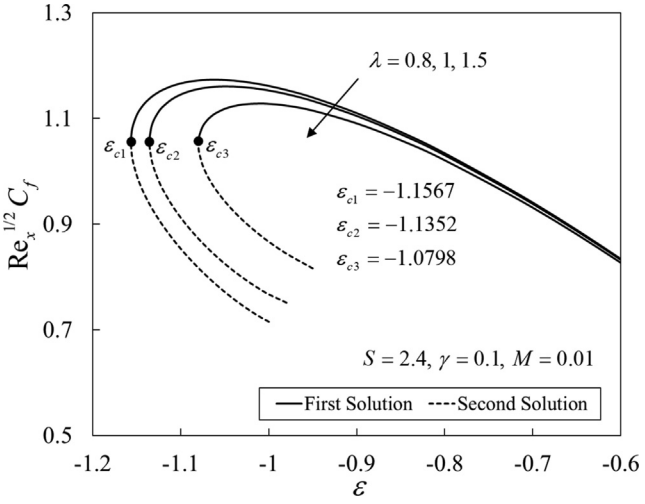

Fig. 4 Skin friction coefficient $Re_x^{1/2}C_f$ vs ε for various values of λ.

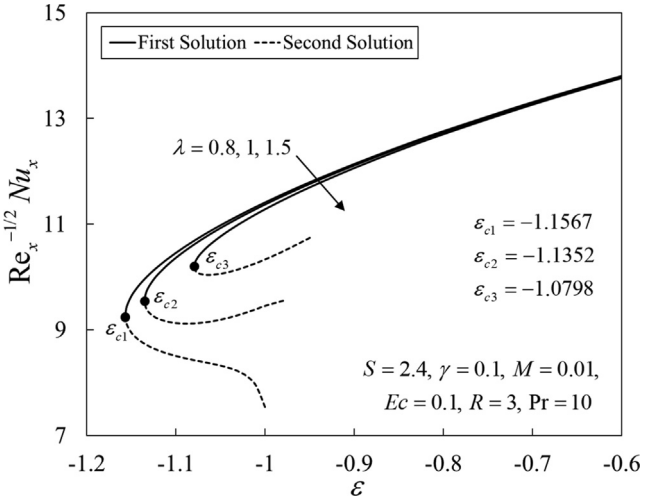

Fig. 5 Local Nusselt number $Re_x^{-1/2}Nu_x$ vs ε for various values of λ.

($M = 0.01$) and $S_{c3} = 2.2901$ ($M = 0.02$). Moreover, the other impact of M is to boost the values of $\mathrm{Re}_x^{1/2}C_f$ and $\mathrm{Re}_x^{-1/2}Nu_x$ with the increasing values of M. Physically, the rising strength of the Lorentz force from the operation of the magnetic field essentially opposes the fluid motion. However, the application of suction helps in stabilizing the unconfined vorticity within the shrinking flow which then tends to induce the skin friction coefficient and simultaneously, enhance the fluid velocity as depicted in Fig. 14 (first solution). Furthermore, the addition of the magnetic parameter also enhances the thermal rate by boosting the heat transfer operation. As earlier stated, the magnetic parameter assists the fluid motion, which synchronously drives the hot particles towards the plate. This active operation augments the heat transfer rate and reduces the temperature (first solution) as shown in Fig. 15.

The impact of Eckert number Ec and radiation parameter R are deliberated in Figs. 10 and 11, respectively. The value of S_c remains unchanged where $S_c = 2.3163$ for each value of Ec and R considered since the Eckert number (arise from the viscous dissipation and Joule heating effect) and thermal radiation parameter does not directly affect the momentum equation (flow progress). However, since these parameters

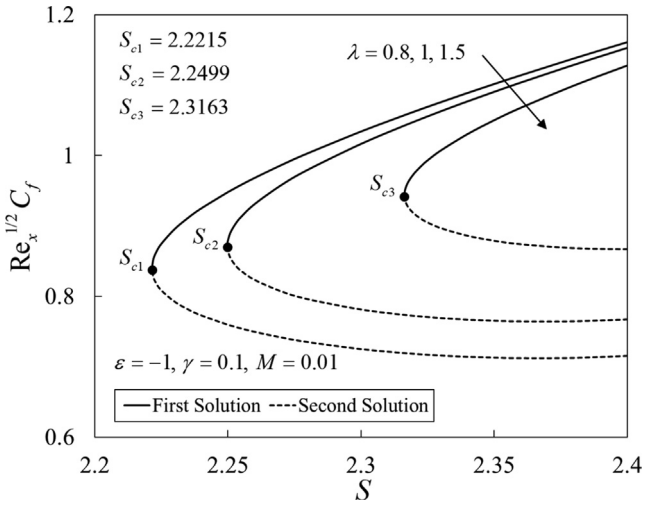

Fig. 6 Skin friction coefficient $Re_x^{1/2}C_f$ vs S for various values of λ.

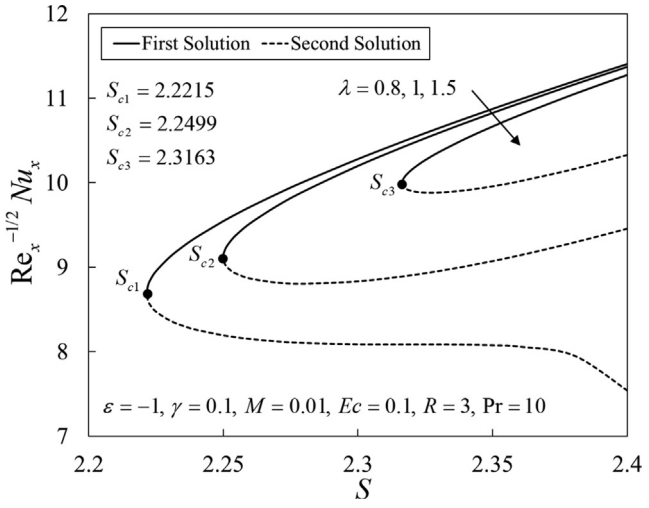

Fig. 7 Local Nusselt number $Re_x^{-1/2}Nu_x$ vs S for various values of λ.

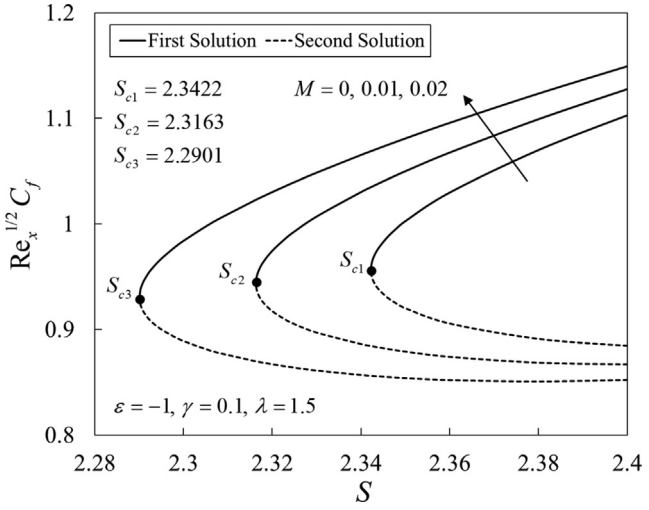

Fig. 8 Skin friction coefficient $Re_x^{1/2}C_f$ vs S for various values of M.

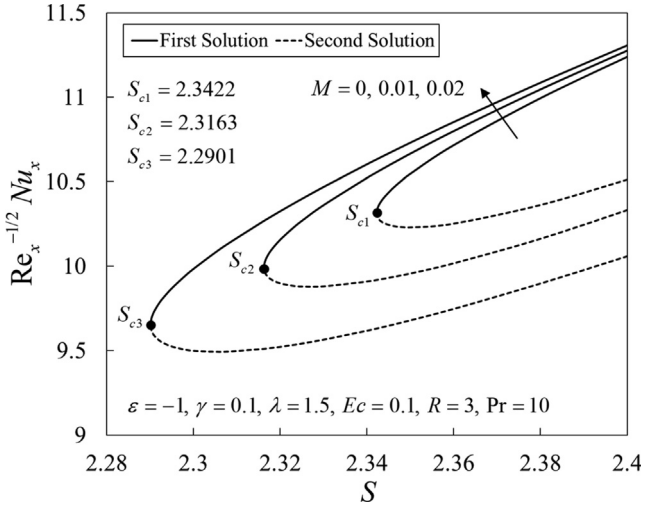

Fig. 9 Local Nusselt number $Re_x^{-1/2}Nu_x$ vs S for various values of M.

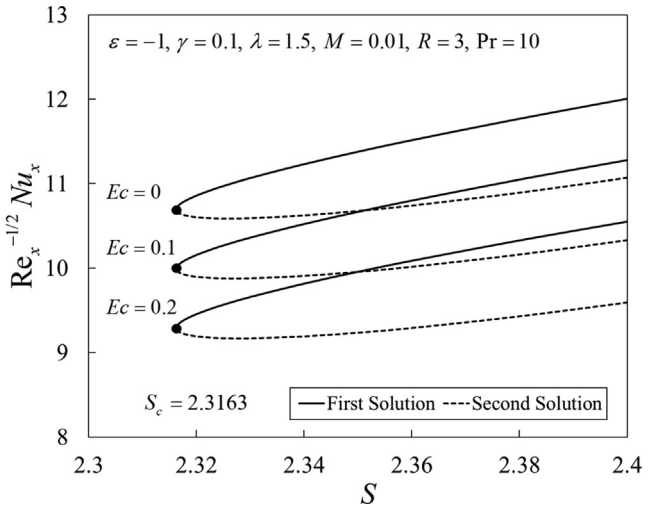

Fig. 10 Local Nusselt number $Re_x^{-1/2}Nu_x$ vs S for various values of Ec.

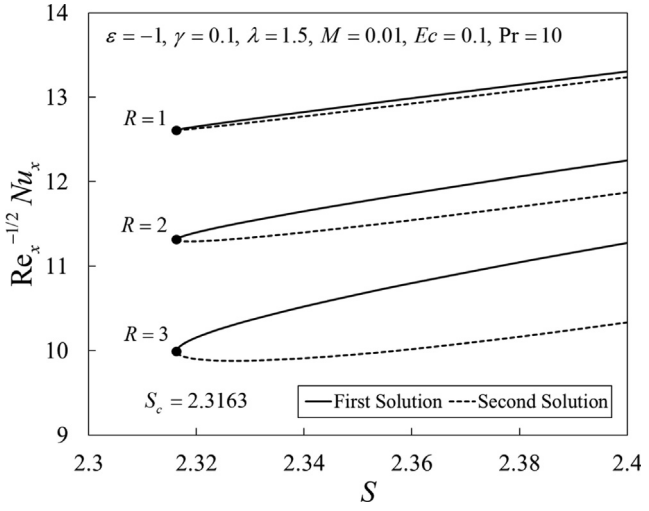

Fig. 11 Local Nusselt number $Re_x^{-1/2}Nu_x$ vs S for various values of R.

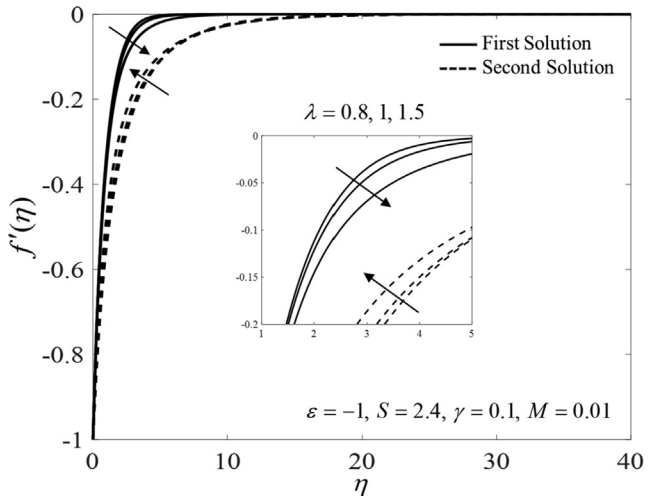

Fig. 12 Velocity profiles $f'(\eta)$ for different values of λ.

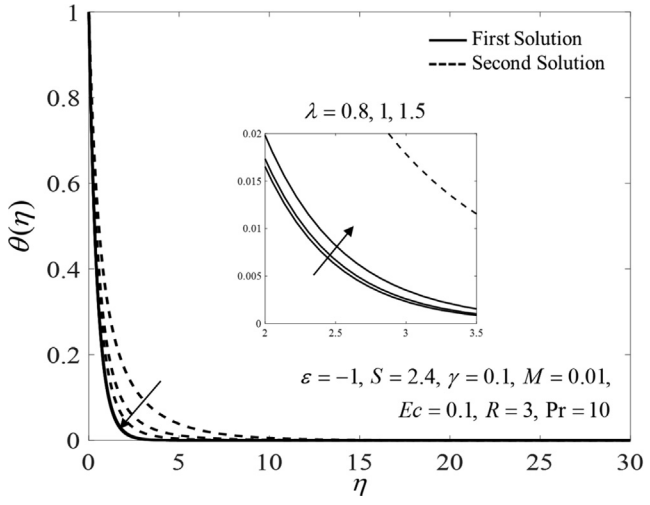

Fig. 13 Temperature profiles $\theta(\eta)$ for different values of λ.

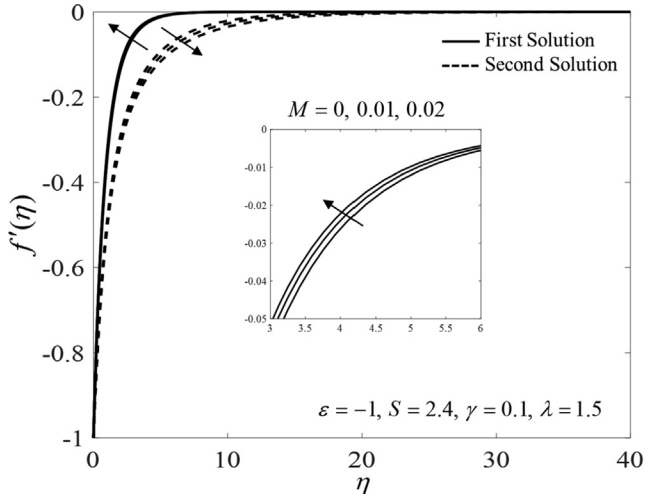

Fig. 14 Velocity profiles $f'(\eta)$ for different values of M.

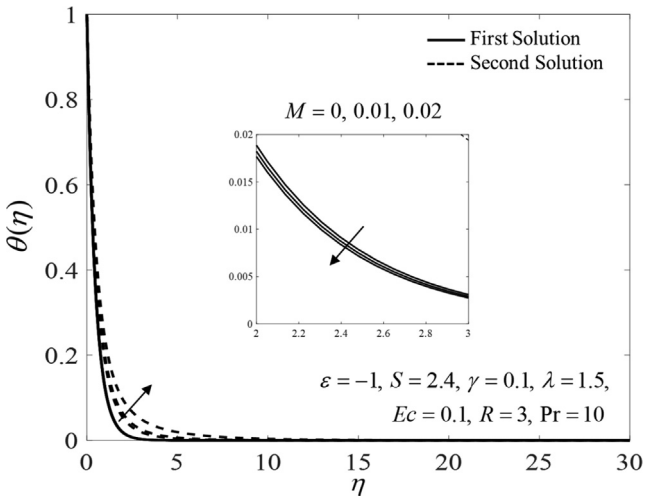

Fig. 15 Temperature profiles $\theta(\eta)$ for different values of M.

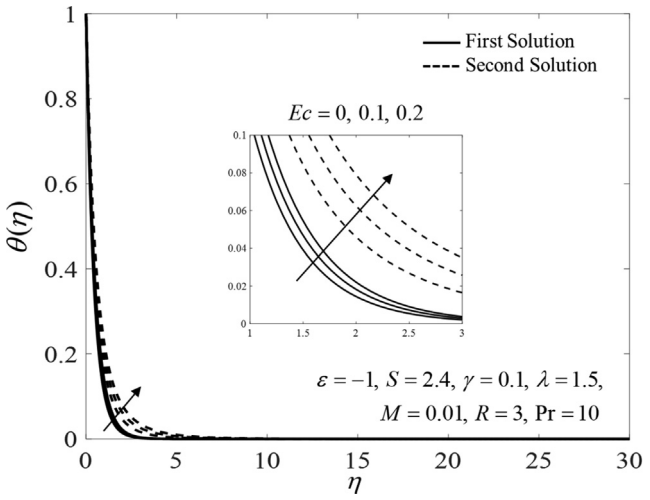

Fig. 16 Temperature profiles $\theta(\eta)$ for different values of Ec.

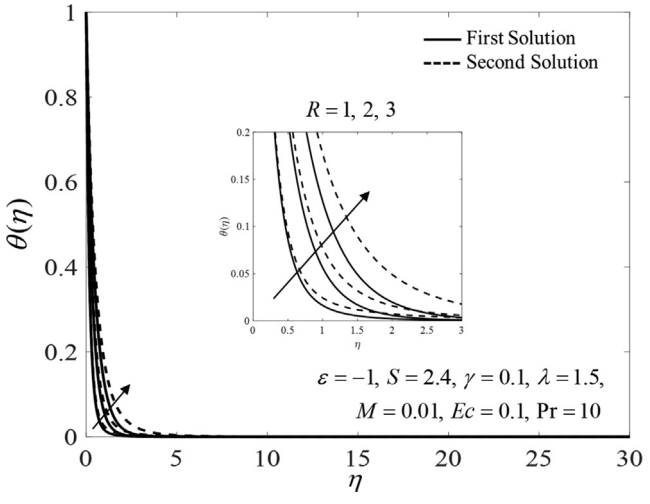

Fig. 17 Temperature profiles $\theta(\eta)$ for different values of R.

are related to the energy equation, it is found that the distribution of $\mathrm{Re}_x^{-1/2}Nu_x$ reduces with the addition of Ec and R. This thermal behaviour is accomplished for both first and second solutions. On the other hand, from Figs. 6–11, it is also observable that the raising in S significantly enhances the distribution of $\mathrm{Re}_x^{1/2}C_f$ $\mathrm{Re}_x^{-1/2}Nu_x$. Physically, the suction parameter can enhance the flow including the skin friction coefficient by restraining the vorticity generation due to the shrinking movement and simultaneously, helps in deferring the boundary layer separation (Miklavčič and Wang [43]). Meanwhile, the increment of thermal rate is related to the progressive movement of the hot fluid particles towards the plate surface.

The obtained dual solutions are also displayed for the distribution of the velocity and the temperature as portrayed in Figs. 12–17 for fixed values of the pertinent parameters. The far-field boundary conditions were satisfied asymptotically. In Fig. 12, as λ increases, the first solution of the fluid velocity decreases while the second solution shows an increment. However, the temperature distribution as displayed in Fig. 13 shows a contradictory behaviour. Figs. 14 and 15 emphasise the impact of the magnetic parameter in enhancing the velocity profile (first solution) while depreciating the temperature profile (first solution). Previous discussion for Figs. 8 and 9 (impact of M on the skin friction and thermal progress) has highlighted the physical reason for this trend. Similar results have been figured out for the variation of Ec and R as depicted evidently in Figs. 16 and 17 where both dual distributions show an ascending trend of the temperature profile. This reflects the reduction of heat transfer operation which synchronously, raises the fluid temperature. Physically, the heat is transmitted from the wall surface to the fluid, and as the radiation parameter increases, the heat transfer rate diminishes which signifies that the fluid temperature near the wall is still hotter than the far-field temperature [70]. Meanwhile, the Eckert number arise from the generation of Joule heating, viscous dissipation and magnetic field effects. These effects physically produces heat from the electric current source to the conducting shrinking plate and simultaneously, increase the temperature [71].

Fig. 18 presents the variation of the smallest eigenvalues α against S where the positive eigenvalue stands for the first solution, while the negative eigenvalue for the second solution.

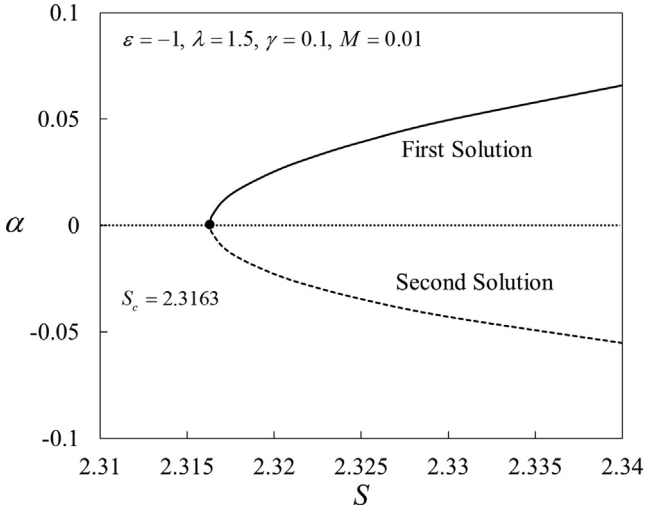

Fig. 18 Eigenvalues α vs mass flux parameter S.

Hence, it can be concluded that the first solution is stable and significantly reliable as time progresses, while the opposite manner is for the second solution.

5. Conclusion

An analysis of radiative heat transfers in a Reiner–Philippoff fluid flow over a nonlinearly shrinking sheet was considered. The effects of magnetohydrodynamics and viscous dissipation were also taken into account. The findings are as follows:

- Dual solutions exist by exerting the suction parameter on the plate surface.
- The Reiner–Philippoff fluid parameter reduces the friction factor and the local Nusselt number due to the obstacles that appear to the shear-thinning phenomenon which reduces fluid interaction with surfaces and generates fewer drag forces.
- The suction and magnetic parameters appears to allow the Reiner–Philippoff fluid molecules to gain control of the surface, resulting in the enhancement of the heat transfer rate.
- The inclusion of Eckert number and thermal radiation parameter reduces the heat transfer performance in the surface domain.
- The stability analysis indicates that the first solution is stable, whereas the second is unstable, as time progresses.

Declaration of Competing Interest

The authors declare that they have no known competing financial interests or personal relationships that could have appeared to influence the work reported in this paper.

Acknowledgments

The authors gratefully acknowledge Universiti Teknikal Malaysia Melaka for the financial support (JURNAL/2019/FTKMP/Q00042). The financial supports were partially received from the Universiti Malaysia Pahang (Project Code: RDU210707).

References

[1] A.P. Deshpande, J.M. Krishnan, P.B.S. Kumar, Rheology of complex fluids, Springer, New York, 2010. doi:10.1007/978-1-4419-6494-6.

[2] J.N. Kapur, R.C. Gupta, Two dimensional flow of Reiner-Philippoff fluids in the inlet length of a straight channel, Appl. Sci. Res. 14 (1) (1964) 13–24.

[3] O.N. Cavatorta, R.D. Tonini, Dimensionless velocity profiles and parameter maps for non-Newtonian fluids, Int. Commun. Heat Mass Transf. 14 (4) (1987) 359–369.

[4] A.G. Hansen, T.Y. Na, Similarity solutions of laminar, incompressible boundary layer equations of non-newtonian fluids, J. Basic Eng. 90 (1968) 71–74, https://doi.org/10.1115/1.3605067.

[5] T.Y. Na, Boundary layer flow of Reiner-Philippoff fluids, Int. J. Non. Linear. Mech. 29 (6) (1994) 871–877, https://doi.org/10.1016/0020-7462(94)90059-0.

[6] M.G. Timol, N.L. Kalthia, Similarity solutions of three-dimensional boundary layer equations of non-Newtonian fluids, Int. J. Non. Linear. Mech. 21 (6) (1986) 475–481.
[7] V. Patel, M.G. Timol, Similarity solutions of the three dimensional boundary layer equations of a class of general non-Newtonian fluids, Int. J. Non. Linear. Mech. 21 (1986) 475–481, https://doi.org/10.1016/0020-7462(86)90043-0.
[8] V.S. Patil, N.S. Patil, M.G. Timol, A remark on similarity analysis of boundary layer equations of a class of non-Newtonian fluids, Int. J. Non. Linear. Mech. 71 (2015) 127–131, https://doi.org/10.1016/j.ijnonlinmec.2014.10.022.
[9] K.S. Yam, S.D. Harris, D.B. Ingham, I. Pop, Boundary-layer flow of Reiner-Philippoff fluids past a stretching wedge, Int. J. Non. Linear. Mech. 44 (10) (2009) 1056–1062, https://doi.org/10.1016/j.ijnonlinmec.2009.08.006.
[10] M.G. Reddy, S. Rani, K.G. Kumar, A.H. Seikh, M. Rahimi-Gorji, E.-S. Sherif, Transverse magnetic flow over a Reiner-Philippoff nanofluid by considering solar radiation, Mod. Phys. Lett. B. 33 (36) (2019) 1950449, https://doi.org/10.1142/S0217984919504499.
[11] M. Gnaneswara Reddy, M.V.V.N.L. Sudharani, K. Ganesh Kumar, A.J. Chamkha, G. Lorenzini, Physical aspects of Darcy-Forchheimer flow and dissipative heat transfer of Reiner-Philippoff fluid, J. Therm. Anal. Calorim. 141 (2) (2020) 829–838, https://doi.org/10.1007/s10973-019-09072-0.
[12] A. Ahmad, Flow of ReinerPhilippoff based nano-fluid past a stretching sheet, J. Mol. Liq. 219 (2016) 643–646, https://doi.org/10.1016/j.molliq.2016.03.068.
[13] A. Ahmad, M. Qasim, S. Ahmed, Flow of Reiner-Philippoff fluid over a stretching sheet with variable thickness, J. Brazilian Soc. Mech. Sci. Eng. 39 (11) (2017) 4469–4473, https://doi.org/10.1007/s40430-017-0840-7.
[14] K.G. Kumar, M.G. Reddy, M.V.V.N.L. Sudharani, S.A. Shehzad, A.J. Chamkha, Cattaneo-Christov heat diffusion phenomenon in Reiner-Philippoff fluid through a transverse magnetic field, Phys. A Stat. Mech. Its Appl. 541 (2020) 123330, https://doi.org/10.1016/j.physa:2019.123330.
[15] P.-Y. Xiong, Y.-M. Chu, M. Ijaz Khan, S.A. Khan, S.Z. Abbas, Entropy optimized Darcy-Forchheimer flow of Reiner-Philippoff fluid with chemical reaction, Comput. Theor. Chem. 1200 (2021) 113222, https://doi.org/10.1016/j.comptc.2021.113222.
[16] T. Sajid, M. Sagheer, S. Hussain, Impact of temperature-dependent heat source/sink and variable species diffusivity on radiative Reiner-Philippoff fluid, Math. Probl. Eng. 2020 (2020) 1–16, https://doi.org/10.1155/2020/9701860.
[17] T. Sajid, S. Tanveer, M. Munsab, Z. Sabir, Impact of oxytactic microorganisms and variable species diffusivity on blood-gold Reiner-Philippoff nanofluid, Appl. Nanosci. 11 (1) (2021) 321–333, https://doi.org/10.1007/s13204-020-01581-x.
[18] G.H.R. Kefayati, Mesoscopic simulation of magnetic field effect on natural convection of power-law fluids in a partially heated cavity, Chem. Eng. Res. Des. 94 (2015) 337–354, https://doi.org/10.1016/j.cherd.2014.08.014.
[19] G.H.R. Kefayati, Magnetic field effect on heat and mass transfer of mixed convection of shear-thinning fluids in a lid-driven enclosure with non-uniform boundary conditions, J. Taiwan Inst. Chem. Eng. 51 (2015) 20–33, https://doi.org/10.1016/j.jtice.2015.01.006.
[20] G.H.R. Kefayati, Double-diffusive natural convection and entropy generation of Bingham fluid in an inclined cavity, Int. J. Heat Mass Transfer 116 (2018) 762–812, https://doi.org/10.1016/j.ijheatmasstransfer.2017.09.065.
[21] G.H.R. Kefayati, R.R. Huilgol, Lattice Boltzmann Method for simulation of mixed convection of a Bingham fluid in a lid-driven cavity, Int. J. Heat Mass Transfer 103 (2016) 725–743, https://doi.org/10.1016/j.ijheatmasstransfer.2016.07.102.
[22] G.H.R. Kefayati, H. Tang, MHD mixed convection of viscoplastic fluids in different aspect ratios of a lid-driven cavity using LBM, Int. J. Heat Mass Transfer 124 (2018) 344–367, https://doi.org/10.1016/j.ijheatmasstransfer.2018.03.083.
[23] G.H.R. Kefayati, H. Tang, Three-dimensional Lattice Boltzmann simulation on thermosolutal convection and entropy generation of Carreau-Yasuda fluids, Int. J. Heat Mass Transfer 131 (2019) 346–364, https://doi.org/10.1016/j.ijheatmasstransfer.2018.11.076.
[24] S. Nandi, B. Kumbhakar, Navier's slip effect on Carreau nanofluid flow past a convectively heated wedge in the presence of nonlinear thermal radiation and magnetic field, Int. Comm. Heat Mass Transfer 118 (2020), https://doi.org/10.1016/j.icheatmasstransfer.2020.104813 104813.
[25] R.P. Sharma, K. Avinash, N. Sandeep, O.D. Makinde, Thermal radiation effect on non-Newtonian fluid flow over a stretched sheet of non-uniform thickness, InDefect and Diffusion Forum 377 (2017) 242–259, Trans Tech Publications Ltd. doi:10.4028/www.scientific.net/DDF.377.242
[26] K.A. Kumar, V. Sugunamma, N. Sandeep, J.R. Reddy, Numerical examination of MHD nonlinear radiative slip motion of non-newtonian fluid across a stretching sheet in the presence of a porous medium, Heat Transf. Res. 50(12) (2019) 1163-1181. doi: 10.1615/HeatTransRes.2018026700
[27] O.A. Abegunrin, I.L. Animasaun, N. Sandeep, Insight into the boundary layer flow of non-Newtonian Eyring-Powell fluid due to catalytic surface reaction on an upper horizontal surface of a paraboloid of revolution, Alex. Eng. J. 57(3) (2018) 2051-60. doi:10.1016/j.aej.2017.05.018
[28] G.S. Seth, A.K. Singha, M.S. Mandal, A. Banerjee, K. Bhattacharyya, MHD stagnation-point flow and heat transfer past a non-isothermal shrinking/stretching sheet in porous medium with heat sink or source effect, Int. J. Mech. Sci. 134 (2017) 98–111, https://doi.org/10.1016/j.ijmecsci.2017.09.049.
[29] G.S. Seth, P.K. Mandal, Analysis of electromagnetohydrodynamic stagnation point flow of nanofluid over a nonlinear stretching sheet with variable thickness, J. Mech. 35 (5) (2019) 719–733, https://doi.org/10.1017/jmech.2019.2.
[30] M.R. Mishra, S.M. Hussain, O.D. Makinde, G.S. Seth, Stability analysis and multiple solutions of a hydromagnetic dissipative flow over a stretching/shrinking sheet, Bul. Chem. Commun. 52 (2020) 259–271, https://doi.org/10.34049/bcc.52.2.5168.
[31] M.J. Babu, N. Sandeep, Effect of nonlinear thermal radiation on non-aligned bio-convective stagnation point flow of a magnetic-nanofluid over a stretching sheet, Alex. Eng. J. 55 (3) (2016) 1931–1939, https://doi.org/10.1016/j.aej.2016.08.001.
[32] N.R.M. Asimoni, N.F. Mohammad, A.R.M. Kasim, S. Shafie, MHD mixed convective flow of power-law nanofluid in a lid-driven cavity with heat generation and chemical reaction effects: Buongiorno's Model, Malaysian J. Fundam Appl. Sci. 16 (2020) 576–584, https://doi.org/10.11113/mjfas.v16n5.1727.
[33] S.M. Zokri, N.S. Arifin, M.K.A. Mohamed, M.Z. Salleh, A.R.M. Kasim, N.F. Mohammad, Influence of radiation and viscous dissipation on magnetohydrodynamic Jeffrey fluid over a stretching sheet with convective boundary conditions, Malaysian J. Fundam Appl. Sci. 13 (2017) 279–284, https://doi.org/10.11113/mjfas.v13n3.621.
[34] I. Waini, A. Ishak, I. Pop, R. Nazar, Dusty hybrid nanofluid flow over a shrinking sheet with magnetic field effects, Int. J. Numer. Methods Heat Fluid Flow. (2021) https://doi.org/10.1108/HFF-01-2021-0081. doi:10.1108/HFF-01-2021-0081.
[35] I. Pop, I. Waini, A. Ishak, MHD stagnation point flow on a shrinking surface with hybrid nanoparticles and melting phenomenon effects, Int. J. Numer. Methods Heat Fluid Flow. (2021) https://doi.org/10.1108/HFF-06-2021-0378. doi:10.1108/HFF-06-2021-0378.

[36] Aurangzaib, A.R.M. Kasim, N.F. Mohammad, S. Shafie, Shafie, Unsteady MHD mixed convection flow of a micropolar fluid along an inclined stretching plate, Heat Transf. - Asian Res. 42 (2) (2013) 89–99, https://doi.org/10.1002/htj.21034.

[37] Aurangzaib, A.R.M. Kasim, N.F. Mohammad, S. Shafie, Shafie, Effect of thermal stratification on MHD free convection with heat and mass transfer over an unsteady stretching surface with heat source, Hall current and chemical reaction, Int. J. Adv. Eng. Sci. Appl. Math. 4 (3) (2012) 217–225, https://doi.org/10.1007/s12572-012-0066-y.

[38] N.S. Arifin, S.M. Zokri, N.A.S. Ariffin, A.R.M. Kasim, M.Z. Salleh, Magnetic field flow of Casson fluid and solid particles with non-linear thermal radiation effect, Malaysian, J. Math. Sci. 14 (2020) 171–184.

[39] N.S. Arifin, S. Mohd Zokri, A.R. Mohd Kasim, M.Z. Salleh, N. F. Mohammad, W.N.S. Wan Yusoff, Aligned magnetic field on dusty Casson fluid over a stretching sheet with Newtonian heating, Malaysian J. Fundam Appl. Sci. 13 (2017) 244–247, https://doi.org/10.11113/mjfas.v13n3.592.

[40] S. Nandi, B. Kumbhakar, G. Shanker Seth, A. J Chamkha, Features of 3D magneto-convective nonlinear radiative Williamson nanofluid flow with activation energy, multiple slips and Hall effect, Phys. Scr. 96 (6) (2021) 065206, https://doi.org/10.1088/1402-4896/abf009.

[41] E.K. Ghiasi, R. Saleh, Analytical and numerical solutions to the 2D sakiadis flow of casson fluid with cross diffusion, inclined magnetic force, viscous dissipation and thermal radiation based on buongiorno's mathematical model, CFD Lett. 11 (2019) 40–54.

[42] N. Gajjela, R. Nandkeolyar, Investigating the magnetohydrodynamic flow of a couple stress dusty fluid along a stretching sheet in the presence of viscous dissipation and suction, Heat Transf. 50 (3) (2021) 2709–2724, https://doi.org/10.1002/htj.22001.

[43] M. Miklavčič, C. Wang, Viscous flow due to a shrinking sheet, Q. Appl. Math. 64 (2) (2006) 283–290, https://doi.org/10.1090/S0033-569X-06-01002-5.

[44] M. Turkyilmazoglu, Dual and triple solutions for MHD slip flow of non-Newtonian fluid over a shrinking surface, Comput. Fluids. 70 (2012) 53–58, https://doi.org/10.1016/j.compfluid.2012.01.009.

[45] L.A. Lund, Z. Omar, I. Khan, J. Raza, E.S.M. Sherif, A.H. Seikh, Magnetohydrodynamic (MHD) flow of micropolar fluid with effects of viscous dissipation and joule heating over an exponential shrinking sheet: Triple solutions and stability analysis, Symmetry (Basel). 12 (2020) 142, https://doi.org/10.3390/sym12010142.

[46] R.I. Yahaya, N. Md Arifin, S.S.P. Mohamed Isa, M.M. Rashidi, Magnetohydrodynamics boundary layer flow of micropolar fluid over an exponentially shrinking sheet with thermal radiation: Triple solutions and stability analysis, Math. Methods Appl. Sci. 44 (13) (2021) 10578–10608.

[47] R.I. Yahaya, N.M. Arifin, S.S.P.M. Isa, Stability analysis on magnetohydrodynamic flow of casson fluid over a shrinking sheet with homogeneous-heterogeneous reactions, Entropy. 20 (2018) 652, https://doi.org/10.3390/e20090652. doi:10.3390/e20090652.

[48] R.I. Yahaya, N. Md Arifin, S.S.P. Mohamed Isa, Stability analysis of MHD Carreau fluid flow over a permeable shrinking sheet with thermal radiation, Sains Malays. 48 (10) (2019) 2285–2295, https://doi.org/10.17576/jsm-2019-4810-25.

[49] I. Waini, A. Ishak, I. Pop, Hiemenz flow over a shrinking sheet in a hybrid nanofluid, Results Phys. 19 (2020) 103351, https://doi.org/10.1016/j.rinp.2020.103351.

[50] I. Waini, A. Ishak, I. Pop, Hybrid nanofluid flow over a permeable non-isothermal shrinking surface, Mathematics. 9 (2021) 538.

[51] I. Waini, A. Ishak, I. Pop, MHD flow and heat transfer of a hybrid nanofluid past a permeable stretching/shrinking wedge, Appl. Math. Mech. (English Ed.). 41 (3) (2020) 507–520.

[52] S. Naramgari, C. Sulochana, MHD flow over a permeable stretching/shrinking sheet of a nanofluid with suction/injection, Alex. Eng. J. 55 (2) (2016) 819–827, https://doi.org/10.1016/j.aej.2016.02.001.

[53] N.S. Anuar, N. Bachok, I. Pop, Numerical computation of dusty hybrid nanofluid flow and heat transfer over a deformable sheet with slip effect, Mathematics. 9 (2021) 643, https://doi.org/10.3390/math9060643.

[54] N.A. Zainal, R. Nazar, K. Naganthran, I. Pop, Heat generation/absorption effect on MHD flow of hybrid nanofluid over bidirectional exponential stretching/shrinking sheet, Chinese, J. Phys. 69 (2021) 118–133, https://doi.org/10.1016/j.cjph.2020.12.002.

[55] N.A. Zainal, R. Nazar, K. Naganthran, I. Pop, MHD flow and heat transfer of hybrid nanofluid over a permeable moving surface in the presence of thermal radiation, Int. J. Numer. Methods Heat Fluid Flow. 31 (3) (2021) 858–879, https://doi.org/10.1108/HFF-03-2020-0126.

[56] N.S. Wahid, N.M. Arifin, N.S. Khashi'ie, I. Pop, Hybrid nanofluid slip flow over an exponentially stretching/shrinking permeable sheet with heat generation, Mathematics. 9 (1) (2021) 30, https://doi.org/10.3390/math9010030.

[57] N.S. Wahid, N.M. Arifin, N.S. Khashi'ie, I. Pop, N. Bachok, M. E.H. Hafidzuddin, Flow and heat transfer of hybrid nanofluid induced by an exponentially stretching/shrinking curved surface, Case Stud, Therm. Eng. 25 (2021) 100982, https://doi.org/10.1016/j.csite.2021.100982.

[58] N.S. Wahid, N.M. Arifin, N.S. Khashi'ie, I. Pop, Marangoni hybrid nanofluid flow over a permeable infinite disk embedded in a porous medium, Int. Commun. Heat Mass Transf. 126 (2021) 105421, https://doi.org/10.1016/j.icheatmasstransfer.2021.105421.

[59] K. Bhattacharyya, G.C. Layek, G.S. Seth, Soret and Dufour effects on convective heat and mass transfer in stagnation-point flow towards a shrinking surface, Phys. Scr. 89 (9) (2014) 095203, https://doi.org/10.1088/0031-8949/89/9/095203.

[60] R.C. Bataller, Similarity solutions for flow and heat transfer of a quiescent fluid over a nonlinearly stretching surface, J. Mater. Process. Technol. 203 (1-3) (2008) 176–183, https://doi.org/10.1016/j.jmatprotec.2007.09.055.

[61] S. Rosseland, Astrophysik und atom-theoretische Grundlagen, Springer-Verlag, Berlin, 1931.

[62] N. Vishnu Ganesh, A.K. Abdul Hakeem, B. Ganga, Darcy-Forchheimer flow of hydromagnetic nanofluid over a stretching/shrinking sheet in a thermally stratified porous medium with second order slip, viscous and Ohmic dissipations effects, Ain Shams Eng. J. 9 (4) (2018) 939–951, https://doi.org/10.1016/j.asej.2016.04.019.

[63] J.H. Merkin, On dual solutions occurring in mixed convection in a porous medium, J. Eng. Math. 20 (2) (1986) 171–179, https://doi.org/10.1007/BF00042775.

[64] P.D. Weidman, D.G. Kubitschek, A.M.J. Davis, The effect of transpiration on self-similar boundary layer flow over moving surfaces, Int. J. Eng. Sci. 44 (11-12) (2006) 730–737, https://doi.org/10.1016/j.ijengsci.2006.04.005.

[65] S.D. Harris, D.B. Ingham, I. Pop, Mixed convection boundary-layer flow near the stagnation point on a vertical surface in a porous medium: Brinkman model with slip, Transp. Porous Media. 77 (2) (2009) 267–285, https://doi.org/10.1007/s11242-008-9309-6.

[66] L.F. Shampine, I. Gladwell, S. Thompson (Eds.), Solving ODEs with MATLAB, Cambridge University Press, 2003.

[67] R. Cortell, Heat and fluid flow due to non-linearly stretching surfaces, Appl. Math. Comput. 217 (19) (2011) 7564–7572, https://doi.org/10.1016/j.amc.2011.02.029.

[68] M. Ferdows, M.J. Uddin, A.A. Afify, Scaling group transformation for MHD boundary layer free convective heat and mass transfer flow past a convectively heated nonlinear radiating stretching sheet, Int. J. Heat Mass Transf. 56 (1-2) (2013) 181–187, https://doi.org/10.1016/j.ijheatmasstransfer.2012.09.020.

[69] I. Waini, A. Ishak, I. Pop, Hybrid nanofluid flow and heat transfer over a nonlinear permeable stretching/shrinking surface, Int. J. Numer. Methods Heat Fluid Flow. 29 (9) (2019) 3110–3127, https://doi.org/10.1108/HFF-01-2019-0057.

[70] N.S. Khashi'ie, N.M. Arifin, N.C. Rosca, A.V. Rosca, I. Pop, Three-dimensional flow of radiative hybrid nanofluid past a permeable stretching/shrinking sheet with homogeneous-heterogeneous reaction, Int. J. Numer. Methods Heat Fluid Flow 32 (2) (2022) 568–588, https://doi.org/10.1108/HFF-01-2021-0017.

[71] N.S. Khashi'ie, N.M. Arifin, I. Pop, Magnetohydrodynamics (MHD) boundary layer flow of hybrid nanofluid over a moving plate with Joule heating, Alexandria Eng. J. 61 (3) (2022) 1938–1945.